



In-situ probing of metallic glass formation and crystallization upon heating and cooling via fast differential scanning calorimetry

S. Pogatscher, P. J. Uggowitzer, and J. F. Löffler


Citation: [Applied Physics Letters](#) **104**, 251908 (2014); doi: 10.1063/1.4884940

View online: <http://dx.doi.org/10.1063/1.4884940>

View Table of Contents: <http://scitation.aip.org/content/aip/journal/apl/104/25?ver=pdfcov>


Published by the [AIP Publishing](#)

Agilent's Electronic Measurement Group is becoming **Keysight Technologies**.



Engineering Education & Research Resources DVD 2014

Agilent is the key to your test and measurement needs **Order yours**

The advertisement features a red header with the text 'Agilent's Electronic Measurement Group is becoming Keysight Technologies.' Below this is a row of icons representing various engineering and research fields: a green Wi-Fi symbol, a blue checkmark, a blue graduation cap, a green book, a yellow sun, a green network diagram, a blue antenna, a purple microchip, a green wave, an orange vertical bar, and a red starburst. To the left of these icons is a DVD disc with the text 'Agilent Technologies Engineering Education & Research Resources DVD 2014'. Below the icons, the text 'Engineering Education & Research Resources DVD 2014' is written in a large, bold, black font. Underneath that, the text 'Agilent is the key to your test and measurement needs' is followed by a red button with the text 'Order yours'. At the bottom of the advertisement is a blue banner with the Agilent Technologies logo and the text 'Agilent Technologies'.

***In-situ* probing of metallic glass formation and crystallization upon heating and cooling via fast differential scanning calorimetry**

S. Pogatscher,^{a)} P. J. Uggowitzer, and J. F. Löffler

Laboratory of Metal Physics and Technology, Department of Materials, ETH Zurich, 8093 Zurich, Switzerland

(Received 15 May 2014; accepted 11 June 2014; published online 24 June 2014)

The crystallization of small-scale Au-based metallic glass samples was investigated by fast differential scanning calorimetry. Rapid cooling and heating makes possible *in-situ* probing of glass formation from the supercooled liquid state or direct transition from the glassy state to the equilibrium liquid and, thereby, the determination of a critical cooling ($\Phi_c \sim 600 \text{ Ks}^{-1}$) and heating rate ($\Phi_h \sim 6 \times 10^3 \text{ Ks}^{-1}$) for crystallization. Crystallization kinetics was studied in the whole supercooled liquid region by linear heating and isothermal calorimetry. We show that the temperature dependence of crystal growth is reflected in a “Kissinger plot” for $\text{Au}_{49}\text{Ag}_{5.5}\text{Pd}_{2.3}\text{Cu}_{26.9}\text{Si}_{16.3}$ and compares well with a model for crystal growth in a glassy system. Linear heating and isothermal measurements after heating the glass show that its crystallization is always growth-controlled up to its temperature of melting. In contrast, for a low degree of direct undercooling from the equilibrium liquid isothermal crystallization is nucleation-controlled, whereas it is again growth-controlled at large undercooling. The overall crystallization behavior of the metallic glass is presented in a complete time-temperature-transformation map on cooling and, so far not accessible, on heating after various cooling procedures. © 2014 AIP Publishing LLC. [<http://dx.doi.org/10.1063/1.4884940>]

The binary Au–Si system was the basis for the first metallic glass production via rapid cooling from the melt.¹ Since then, intensive research on this class of materials has led to the discovery of numerous metallic glass-forming systems.² High strength, hardness and elastic strain limit, good soft-magnetic properties, excellent corrosion resistance, homogeneity and isotropy on a small scale, and viscous flow workability in the supercooled liquid region are unique properties of metallic glasses.^{3–6} In particular, bulk metallic glasses developed from the Au-based system^{7–9} are of great interest for the production of small-scale devices¹⁰ (e.g., micro-electro-mechanical systems, micro-robotics, micro-manipulators) because of their good glass-forming ability, low glass transition temperature, wide supercooled liquid region, and oxidation resistance. Various production techniques such as imprinting, embossing, micro-replication, and micro-molding have been tested and may soon enter large-scale production.^{11,12} However, more knowledge about crystallization kinetics in the supercooled liquid region is necessary for all these net-shape thermoplastic-forming processes. Unfortunately, the rapid crystallization of metallic glasses limits most experimental studies in the supercooled liquid region.^{4–6}

Using conventional thermo-analytical methods (i.e., differential scanning calorimetry, DSC), it is impossible to realize controlled constant heating or cooling rates much higher than a few Ks^{-1} . However, the development of chip-based calorimeters in the last few years^{13,14} enables measurements at rates which are orders of magnitude higher. Heating and cooling with several 10^4 Ks^{-1} and 10^3 Ks^{-1} , respectively, can be realized with the recently available first commercial instrument.¹⁵ The device has already been utilized in the polymer community and was recently applied to phase-

change materials.^{16,17} Au-based bulk metallic glasses seem ideal candidates for investigation by this device because they exhibit a low liquidus temperature. Fast DSC (FDSC) is interesting not only because *in-situ* probing of the glass formation and crystallization behavior in the whole supercooled liquid region seems possible but also with respect to the comparable sample scale to thermoplastic processing of small-scale devices made from these metallic glasses. Still at its beginning, the method is expected to become a standard in thermal analysis of metallic glasses.

Here, we *in-situ* probe the well-known bulk metallic glass $\text{Au}_{49}\text{Ag}_{5.5}\text{Pd}_{2.3}\text{Cu}_{26.9}\text{Si}_{16.3}$ ⁷ and document an investigation of crystallization kinetics in the whole super-/undercooled liquid region up to the temperature of melting. We discuss the temperature dependence of crystal growth and present DSC curves, where the metallic glass transforms from its glassy state directly to the equilibrium liquid without detectable crystallization. Such DSC curves have so far not been reported for metallic systems. We also present a complete time-temperature-transformation (TTT) diagram upon heating of a metallic glass.

The elements Au (99.95%), Cu (99.9%), Ag (99.5%), Si (99.95%), and Pd (99.95%) were pre-alloyed in a sealed quartz tube under Ar atmosphere (purity: 99.999% for all used gases) by repeated induction melting.¹⁸ To obtain chemically homogeneous and thin samples, glassy ribbons of $\sim 10 \mu\text{m}$ thickness were produced by melt spinning under He atmosphere. The atomic structure of the ribbons was confirmed to be amorphous by X-ray diffraction (not shown here). Conventional thermal analysis was performed in a differential scanning calorimeter (DSC 1 by Mettler-Toledo) at a heating rate of 0.17 Ks^{-1} under Ar atmosphere at a flow rate of 30 ml min^{-1} . FDSC was performed in power compensation mode using a Mettler-Toledo Flash-DSC 1. The sample support temperature of the FDSC was set to 183 K using a Huber intracooler TC90. The

^{a)}Electronic mail: Stefan.Pogatscher@mat.ethz.ch

furnace was purged with Ar at a flow rate of 10 ml min^{-1} . FDSC samples were prepared by cutting the melt-spun ribbons under a stereomicroscope to small pieces of $<100 \times 100 \mu\text{m}^2$ (see inset to Fig. 1(a)). The mass of the FDSC samples was determined using the enthalpy of melting (H_m) measured by conventional DSC (40.4 Jg^{-1}) as a reference value.

Figure 1 shows typical FDSC scans for a $\text{Au}_{49}\text{Ag}_{5.5}\text{Pd}_{2.3}\text{Cu}_{26.9}\text{Si}_{16.3}$ sample with a mass of $2 \mu\text{g}$. The insets illustrate the applied temperature-time programs and also show a micrograph of a sample on the sensor (inset to Fig. 1(a)). To melt the sample, it was held for 10 s at 723 K. Longer holding times or higher temperatures (up to 773 K, which were achieved for some sensors) were confirmed not to influence the results. This illustrates no aging, oxidation, or reaction of the sample in contact with the sensor. Reproducibility after a series of measurements was very good, as was judged by comparing thermal cycles at the start and end of each measurement series. Figure 1(a) shows curves for the heat flow measured during cooling from the melt with rates of 10 Ks^{-1} up to $5 \times 10^3 \text{ Ks}^{-1}$. A transition from crystallization in the supercooled liquid region to *in-situ* amorphization is observed at around 600 Ks^{-1} (Φ_c). The crystallization peak shifts to lower temperature, and

the enthalpy of crystallization (H_c) decreases with increasing cooling rate until the crystallization peak vanishes at 600 Ks^{-1} . Note that the signal generally scales with the cooling rate, because the curves in Fig. 1 are not normalized to the rate (height of crystallization peaks decreases with decreasing rate for $\Phi \ll \Phi_c$). A clear glass transition, dependent on the cooling rate, is also observed. The Φ_c found falls conveniently into the optimal working range of the FDSC device. An estimate from the critical casting thickness reported for $\text{Au}_{49}\text{Ag}_{5.5}\text{Pd}_{2.3}\text{Cu}_{26.9}\text{Si}_{16.3}$ ⁷ suggests a somewhat lower value of around 100 Ks^{-1} . Although this is not a large deviation in view of an estimation from the critical casting thickness,¹⁹ we briefly discuss possible influences. A reaction with the sensor membrane material is unlikely, because Φ_c was confirmed to be similar for different membrane surface materials such as silicon nitride, silicon oxide or graphite, and is also reproducible after many scans. Another reason may be the high surface/volume ratio for small-scale samples, because it has been reported that $\text{Au}_{49}\text{Ag}_{5.5}\text{Pd}_{2.3}\text{Cu}_{26.9}\text{Si}_{16.3}$ crystallizes easily at the surface.^{20,21} Although small, such an effect would need to be considered in thermoplastic forming of small-scale devices and is subject of our further studies.

Heating the glassy samples after cooling the melt at the maximum achievable cooling rate of $5 \times 10^3 \text{ Ks}^{-1}$ showed a clear glass transition and, at low to medium rates, crystallization in the supercooled liquid state (Fig. 1(b)). The crystallization peak in Fig. 1(b) shifts to higher temperatures for increasing heating rates until it merges with the melting peak. For rates higher than around $6 \times 10^3 \text{ Ks}^{-1}$ neither crystallization nor melting are visible and a direct transition from the supercooled to the equilibrium liquid occurs without any detectable heat flow, so far not measured for metallic systems. It is expected that Φ_h will be higher than Φ_c , because the maximum in the nucleation rate appears to be at a lower temperature than the maximum in the growth rate for metallic glasses.²² However, such a high Φ_h value has not previously been reported for a metallic glass because it has simply not been accessible.

The temperature of melting (T_m) is known to be independent of the heating rate. Nevertheless, at high heating rates, a shift of the onset to higher temperatures is seen in Fig. 1(b). This is due to a thermal lag between sensor and sample, and needs to be corrected when the kinetics of crystallization is studied at high heating rates. A linear function on the heating rate can be used for this purpose,²³ and is illustrated in the following. Figure 2 shows the onset of melting as a function of the heating rate. Note that crystalline samples were used for all thermal lag corrections to avoid the effect of the merging of crystallization and melting close to Φ_h and to access higher rates than Φ_h . The inset to Fig. 2 shows the melting peak obtained from a conventional DSC measurement. The onset of melting obtained by FDSC deviates by $\leq 8 \text{ K}$, which is most likely due to the absolute temperature accuracy of the chip sensors and can be easily corrected. Temperature values from FDSC experiments deployed to analyze crystallization kinetics are therefore corrected by the function $\Delta T_{\text{corr}} = k\Phi + (618 \text{ K} - d)$, where k is the thermal lag ($2.3 \times 10^{-3} \text{ s}$ in Fig. 2) and d is the onset of melting at 0.16 Ks^{-1} calculated from FDSC measurements (610 K in Fig. 2).

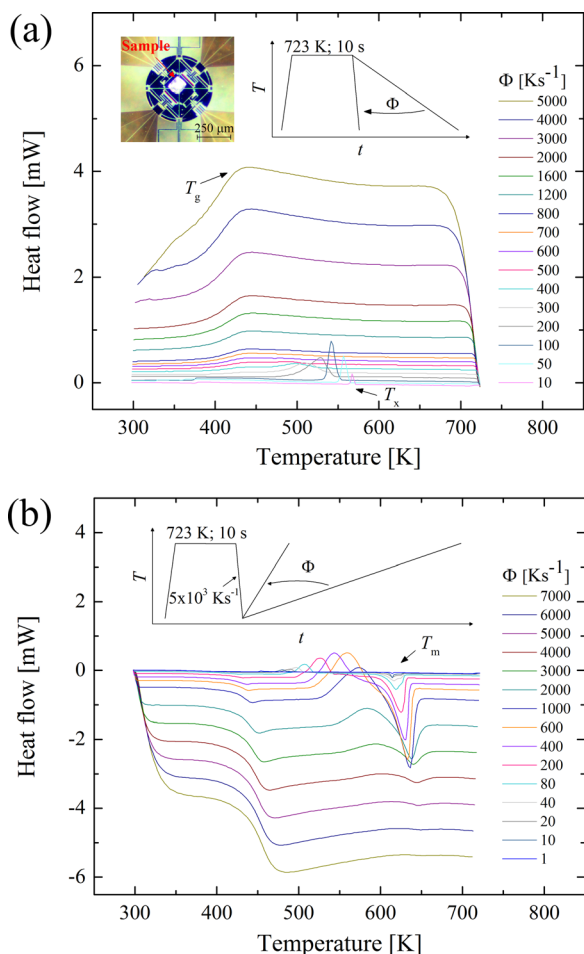


FIG. 1. Typical FDSC scans for a $\text{Au}_{49}\text{Ag}_{5.5}\text{Pd}_{2.3}\text{Cu}_{26.9}\text{Si}_{16.3}$ metallic glass with a mass of $2 \mu\text{g}$. (a) Cooling from the melt at 723 K at rates of 10 Ks^{-1} to $5 \times 10^3 \text{ Ks}^{-1}$. (b) Heating the metallic glass to the equilibrium liquid with rates of 1 Ks^{-1} to $7 \times 10^3 \text{ Ks}^{-1}$. Insets in (a) and (b) illustrate the applied temperature-time programs, and a micrograph of a sample on the sensor is shown in (a).

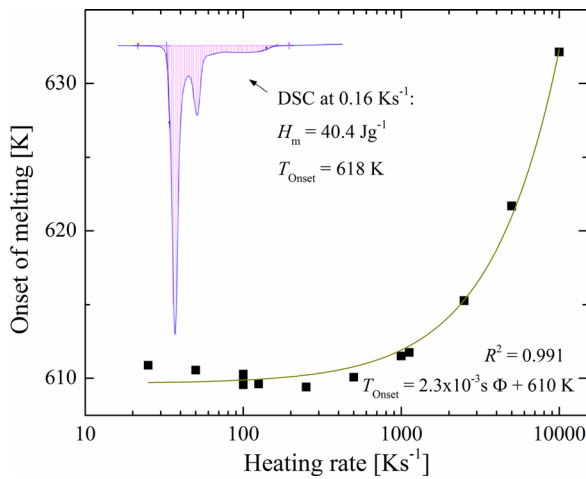


FIG. 2. Onset of melting measured at heating rates of up to 10^4 Ks^{-1} for a crystalline sample with a mass of $2 \mu\text{g}$. The yellow line is a linear fit in the T_{Onset} vs. $\log(\Phi)$ representation. The inset shows the melting peak measured by conventional DSC.

Figure 3(a) shows a Kissinger plot²⁴ of the crystallization peak upon heating a fully amorphous $\text{Au}_{49}\text{Ag}_{5.5}\text{Pd}_{2.3}\text{Cu}_{26.9}\text{Si}_{16.3}$ sample (cooled at $5 \times 10^3 \text{ Ks}^{-1}$). Plotting $\ln(\Phi/T_p^2)$ versus $1/T_p$ should in the case of crystal growth give a slope of $-Q/R$, where T_p is the peak temperature of the crystallization exotherm, Q is the effective activation energy for crystallization, and R is the gas constant. For conventional DSC measurements, only low heating rates are accessible, and the Kissinger plot was found to be a straight line for

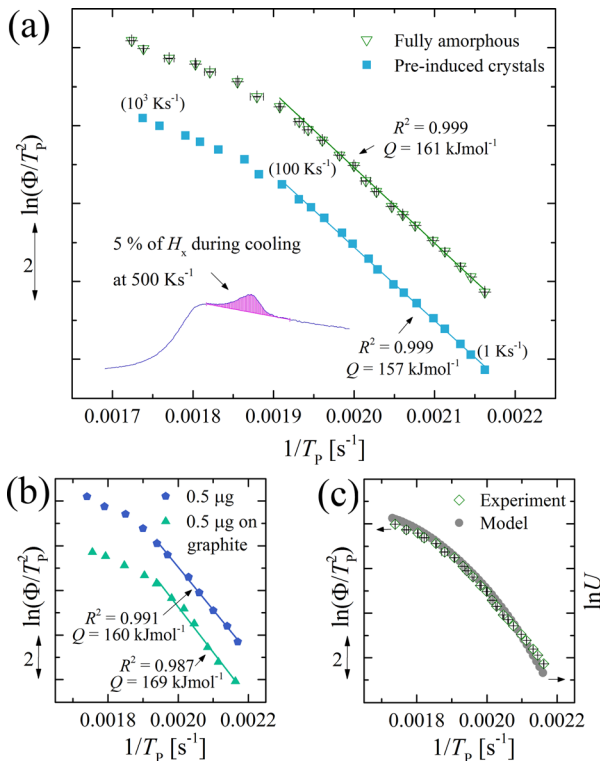


FIG. 3. Kissinger plot. (a) Experimental results for a fully amorphous sample with a mass of $2 \mu\text{g}$ and a sample with pre-induced crystals (5% crystallization, see inset) with a mass of $2 \mu\text{g}$. (b) Results for a different sample mass ($0.5 \mu\text{g}$) and sensor surface (graphite). Lines in the range of 1 Ks^{-1} to 100 Ks^{-1} are fits to the data using Kissinger analysis. (c) Comparison of the experimental results from a fully amorphous sample with a mass of $2 \mu\text{g}$ and a theoretically predicted temperature dependence of crystal growth (Eq. (1)).

$\text{Au}_{49}\text{Ag}_{5.5}\text{Pd}_{2.3}\text{Cu}_{26.9}\text{Si}_{16.3}$, with $Q = 162 \text{ kJmol}^{-1}$ attributed to an activation energy for diffusion.²⁵

Such effective activation energy deduced from linear heating experiments was linked to crystal growth²⁶ for glassy systems, because nuclei are expected to form already at low temperatures near the glass transition because of the deep undercooling. Although from Fig. 3(a) we can deduce a similar effective activation energy (161 kJmol^{-1}) with a good linear correlation between 1 and 100 Ks^{-1} (linear fits in this heating rate range are shown for comparison in Fig. 3), we see clearly that all lines are curved (visible for $\Phi > 100 \text{ Ks}^{-1}$). Note that the Kissinger plot appears similar if a different mass ($0.5 \mu\text{g}$) or another sensor surface material (graphite) is used (Fig. 3(b)).

A curved Kissinger plot was also found in Ref. 16 and attributed to the temperature dependence of crystal growth for the phase-change material $\text{Ge}_2\text{Sb}_2\text{Te}_5$ (GST). Although GST shows no local composition change upon crystallization and is not directly comparable, the observed behavior may be the same as that of our metallic glass. Fig. 3(a) also shows data for a sample which was cooled slightly below the critical cooling rate to introduce a small fraction of crystals to the sample prior to heating the sample in the FDSC device (5% of the crystallization enthalpy, H_x , is detected near the glass transition; see the inset to Fig. 3(a)). Interestingly, the same temperature dependence as for a fully amorphous sample is observed, which is a good indicator that the Kissinger plot reflects the temperature dependence of crystal growth.

The trend of a curved plot can be understood by looking at the theoretical temperature dependence of crystal growth in a glassy system,²⁷

$$U(T) = U_{\text{kin}} \times (1 - \exp(-\Delta G/RT)), \quad (1)$$

where ΔG is the Gibbs free energy difference between the melt and crystal and U_{kin} is the kinetic coefficient of crystal growth. The free energy difference ΔG can be easily calculated by integrating the specific heat functions of the liquid and crystalline phases measured in Ref. 28 and applying the procedure given in Ref. 29. The coefficient U_{kin} can be linked to the viscosity (η) via $U_{\text{kin}} \sim \eta^{-1}$, which approximates the Stokes-Einstein relationship between diffusivity and viscosity for growth governed by diffusion processes at the liquid-crystal interface.³⁰ Note that $D\eta = \text{const}$ has been recently confirmed for dense liquids.³¹ The temperature dependence of η can be described by the well-known Vogel-Fulcher-Tammann (VFT) relation,

$$\eta(T) = A \exp(B/(T - T_0)), \quad (2)$$

where T_0 is the VFT temperature. Using the values for the VFT parameters in Ref. 25 for $\text{Au}_{49}\text{Ag}_{5.5}\text{Pd}_{2.3}\text{Cu}_{26.9}\text{Si}_{16.3}$ ($A = 3.855 \times 10^{-5} \text{ Pa s}$, $B = 4184 \text{ K}$, and $T_0 = 273.5 \text{ K}$), we can calculate the temperature dependence of U and compare it to the experimental data in the Kissinger plot (Fig. 3(c)). Excellent agreement with the measurement is found. Although this simple theoretical treatment of diffusion-controlled crystal growth of a planar interface does not take into account possible long-range diffusion or decoupling of viscosity from diffusion,²⁷ it reproduces the experimental data well and, thus, indicates that the Kissinger plot

expresses the temperature dependence of crystal growth for this metallic glass.

The crystallization behavior can also be studied *in-situ* via FDSC by performing isothermal measurements to record TTT diagrams^{30,32} for different thermal histories (Fig. 4). The temperature programs applied in this study are shown in the inset to Fig. 4. We present the first complete TTT diagram on heating for metallic glasses. Note that the data points in Fig. 4 represent the peak values: it was experimentally impossible to extract accurate values for the onset of crystallization for all temperatures. Analogous to the Kissinger plot for linear heating, the melt was quenched to 298 K at a rate of $5 \times 10^3 \text{ Ks}^{-1}$ (fully amorphous state), or cooled slightly below the critical cooling rate at $5 \times 10^2 \text{ Ks}^{-1}$ (pre-induced crystals; 5% of H_x ; see Fig. 3(a)), and then heated at a rate of 10^4 Ks^{-1} ($> \Phi_h$) to the temperature of the isothermal measurement. Crystallization is faster for the sample with pre-induced crystals, but both TTT-curves on heating exhibit similar temperature dependencies as it was observed for linear heating in Fig. 3(a).

Isothermal scans were also performed directly after cooling at a rate of $5 \times 10^3 \text{ Ks}^{-1}$ to the desired temperature to record the TTT diagram on cooling from the melt (see Fig. 4). Again, a typical C-shape is obtained, but with a different temperature dependence of crystallization. The TTT-curves of the fully amorphous samples on heating and on cooling merge at the low-temperature branches of the C-curves, but diverge at high temperatures. Upon heating from low temperature, nuclei are expected to form already near the glass transition, due to deep undercooling, and the crystallization peak, thus, mainly corresponds to growth.²⁶ This agrees well with the isothermal results from the sample with pre-induced crystals (Fig. 4) and the Kissinger plot in Fig. 3. It remains valid even when heating the fully amorphous sample at a rate of 10^4 Ks^{-1} , which is significantly above the rate where crystallization can be detected during linear heating (around $6 \times 10^3 \text{ Ks}^{-1}$). Due to the fact that the low-temperature branches of the isothermal TTT diagrams merge on heating and cooling, we assume that crystallization in general is limited by growth in the low-temperature region for $\text{Au}_{49}\text{Ag}_{5.5}\text{Pd}_{2.3}\text{Cu}_{26.9}\text{Si}_{16.3}$. At increasing temperature,

crystallization on heating remains growth-controlled with increasing atomic mobility, but the growth kinetics slows down due to an ever-decreasing ΔG (see Eq. (1)) near the temperature of melting. At 540 K, the C-curve on cooling diverges from that on heating. In the case of cooling, nucleation becomes rate-limiting for crystallization at high temperatures, because there the nuclei have to form at low undercooling, i.e., according to classical nucleation theory, with a low driving force. Crystallization above the nose of the TTT-diagram thus occurs upon cooling at much longer time scales than upon heating, which is nicely seen in Fig. 4.

In summary, we have shown that crystallization of small-scale metallic glass samples can be investigated *in-situ* by fast differential scanning calorimetry in the whole super-/undercooled liquid region. Linear heating with high rates and the Kissinger plot provide significant experimental insights into the temperature dependence of crystal growth in metallic glasses in a temperature range which has not been investigated previously. We presented the first DSC scan upon linear heating from the supercooled liquid to the equilibrium liquid of a metallic system without detectable heat flow, i.e., without crystallization or melting. The critical heating rate Φ_h of $\text{Au}_{49}\text{Ag}_{5.5}\text{Pd}_{2.3}\text{Cu}_{26.9}\text{Si}_{16.3}$ for reaching the equilibrium liquid without crystallization was measured to be $6 \times 10^3 \text{ Ks}^{-1}$, whereas the critical cooling rate Φ_c for amorphization was found to be one order of magnitude lower. We also measured the complete time-temperature-transformation diagrams of this Au-based metallic glass upon cooling and upon heating. We find that linear heating and isothermal experiments after heating always generate growth-controlled crystallization up to the temperature of melting, whereas isothermal crystallization after direct undercooling of the melt is growth-controlled at low temperature but nucleation-controlled at high temperature. This difference in crystallization behavior can be well explained by classical nucleation and growth theory.

The authors thank Fabio Krogh at LMPT and Jürgen Schawe at Mettler Toledo AG for fruitful discussions, and Eva Sediva for preliminary work using the FDSC. Support by the Swiss National Science Foundation (SNF Grant No. 200020-135100) is gratefully acknowledged.

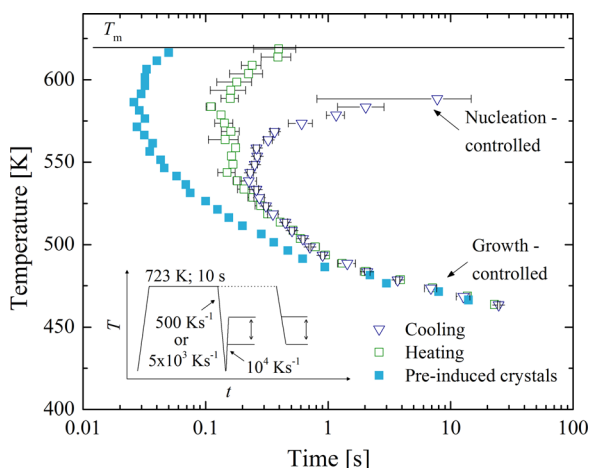


FIG. 4. Isothermal TTT-diagrams measured upon heating from the amorphous and semi-crystalline states and measured upon cooling directly from the equilibrium melt. The inset illustrates the temperature-time programs applied.

¹W. Klement, R. H. Willens, and P. Duwez, *Nature* **187**, 869 (1960).

²C. Suryanarayana and A. Inoue, *Bulk Metallic Glasses* (Taylor & Francis CRC Press, 2010), p. 1.

³A. L. Greer, *Science* **267**, 1947 (1995).

⁴W. L. Johnson, *MRS Bull.* **24**, 42 (1999).

⁵A. Inoue, *Acta Mater.* **48**, 279 (2000).

⁶J. F. Löffler, *Intermetallics* **11**, 529 (2003).

⁷J. Schroers, B. Lohwongwatana, W. L. Johnson, and A. Peker, *Appl. Phys. Lett.* **87**, 061912 (2005).

⁸W. Zhang, H. Guo, M. W. Chen, Y. Saotome, C. L. Qin, and A. Inoue, *Scr. Mater.* **61**, 744 (2009).

⁹H. Guo, W. Zhang, M. W. Chen, Y. Saotome, M. Fukuhara, and A. Inoue, *Metall. Mater. Trans. A* **42**, 1486 (2011).

¹⁰G. Kumar, A. Desai, and J. Schroers, *Adv. Mater.* **23**, 461 (2011).

¹¹G. Kumar, H. X. Tang, and J. Schroers, *Nature* **457**, 868 (2009).

¹²Y. C. Chen, J. P. Chu, J. S. C. Jang, and C. W. Wu, *Mater. Sci. Eng., A* **556**, 488 (2012).

¹³E. Zhuravlev and C. Schick, *Thermochim. Acta* **505**, 1 (2010).

¹⁴E. Zhuravlev and C. Schick, *Thermochim. Acta* **505**, 14 (2010).

- ¹⁵V. Mathot, M. Pyda, T. Pijpers, G. V. Poel, E. Van De Kerkhof, S. Van Herwaarden, F. Van Herwaarden, and A. Leenaers, *Thermochim. Acta* **522**, 36 (2011).
- ¹⁶J. Orava, A. L. Greer, B. Gholipour, D. W. Hewak, and C. E. Smith, *Nature Mater.* **11**, 279 (2012).
- ¹⁷J. Orava, A. L. Greer, B. Gholipour, D. W. Hewak, and C. E. Smith, *Appl. Phys. Lett.* **101**, 091906 (2012).
- ¹⁸S. Mozgovoy, J. Heinrich, U. E. Klotz, and R. Busch, *Intermetallics* **18**, 2289 (2010).
- ¹⁹J. F. Löffler, A. A. Kündig, and F. H. D. Torre, in *Materials Processing Handbook*, edited by J. R. Groza, J. F. Shackelford, E. J. Lavernia, and M. T. Powers (Taylor & Francis CRC Press, 2007), pp. 1–17.
- ²⁰S. V. Ketov, N. Chen, A. Caron, A. Inoue, and D. V. Louzguine-Luzgin, *Appl. Phys. Lett.* **101**, 241905 (2012).
- ²¹S. Mechler, E. Yahel, P. S. Pershan, M. Meron, and B. Lin, *Appl. Phys. Lett.* **98**, 251915 (2011).
- ²²J. Schroers, A. Masuhr, W. L. Johnson, and R. Busch, *Phys. Rev. B* **60**, 11855 (1999).
- ²³B. Zhao, J. Zhao, W. Zhang, B. Yang, Q. Zhai, C. Schick, and Y. Gao, *Thermochim. Acta* **565**, 194 (2013).
- ²⁴H. E. Kissinger, *Anal. Chem.* **29**, 1702 (1957).
- ²⁵G. Fiore, I. Ichim, and L. Battezzati, *J. Non-Cryst. Solids* **356**, 2218 (2010).
- ²⁶K. F. Kelton, *Mater. Sci. Eng., A* **226–228**, 142 (1997).
- ²⁷M. D. Ediger, P. Harrowell, and L. Yu, *J. Chem. Phys.* **128**, 034709 (2008).
- ²⁸G. D. Fontana, G. L. Fiore, and L. Battezzati, *J. Non-Cryst. Solids* **382**, 95 (2013).
- ²⁹R. Busch, Y. J. Kim, and W. L. Johnson, *J. Appl. Phys.* **77**, 4039 (1995).
- ³⁰J. F. Löffler, J. Schroers, and W. L. Johnson, *Appl. Phys. Lett.* **77**, 681 (2000).
- ³¹J. Brillo, A. I. Pommrich, and A. Meyer, *Phys. Rev. Lett.* **107**, 165902 (2011).
- ³²J. Schroers, Y. Wu, R. Busch, and W. L. Johnson, *Acta Mater.* **49**, 2773 (2001).